Deep Space Network

202
Doppler Tracking

Document Owner:		Approved by:	
Signature Provided	01/08/2019	Signature Provided	01/10/2019
Andrew O'Dea Telemetry, Tracking, and Command System Engineer	Date	Timothy T. Pham Communications Systems Chief Engineer	Date
Prepared By:		**Released by:**	
Signature Provided	12/18/2018	Signature Provided	01/15/2019
Peter Kinman Telecommunications Technical Consultant	Date	Christine Chang DSN Document Release Authority	Date

DSN No. **810-005, 202, Rev. C**
Issue Date: January 22, 2019
JPL D-19379; CL#19-0432

Jet Propulsion Laboratory
California Institute of Technology

Users must ensure that they are using the current version in DSN Telecommunications Link Design Handbook website:
https://deepspace.jpl.nasa.gov/dsndocs/810-005/

Review Acknowledgment

By signing below, the signatories acknowledge that they have reviewed this document and provided comments, if any, to the signatories on the Cover Page.

Signature Provided	12/20/2018	Signature Provided	01/09/2019
Jeff B. Berner DSN Project Chief Engineer	Date	Dong K. Shin DSN System Engineer	Date

Signature not provided	
Scott Bryant DSN Ranging Cognizant Development Engineer	Date

Document Change Log

Rev	Issue Date	Prepared By	Affected Sections or Pages	Change Summary
Initial	11/30/2000	P. W. Kinman	All	New Module
A	12/15/2002	P. W. Kinman	Many	Added Discussion of one-way Doppler error and X-Up/S-Down Solar Phase Scintillation errors. Renumbered all equations.
B	9/30/2010	D. K. Shin	All	Replaced DSMS with DSN. Eliminated the Rev. E designation for the document series.
C	01/22/2019	P. W. Kinman	All	Title of module changed to “Doppler Tracking”. Added new equation on data imbalance. Added new equations on uplink noise affecting coherent operation. Added new equations on the effect of phase noise. Equations on phase scintillation corrected. Added Appendix A, “Carrier-Loop Transfer Function,” and Appendix B, “Glossary of Parameters”. Figures 3, 4, 5, 11, 12, and 13 added. Several sections were rewritten for better clarity.

Contents

Illustrations

Figure **Page**

Tables

Table **Page**

1. Introduction

1.1 Purpose

This module provides sufficient information for the telecommunications engineer to understand the capabilities and limitations of the equipment used for Doppler measurement at the Deep Space Network (DSN).

1.2 Scope

The scope of this module is limited to those features of the Downlink Channel at the 34-m High-efficiency (34-m HEF), 34-m Beam Waveguide (34-m BWG), and 70-m stations that relate to the measurement of and reporting of the Doppler effect.

2. General Information

The relative motion of a transmitter and receiver causes the received carrier frequency to differ from that of the transmitter. This Doppler shift depends on the range rate—the rate-of-change of the distance separating transmitter and receiver. In the DSN a Doppler measurement consists of a set of carrier phase measurements. From these phase data, frequency may be calculated, since frequency is the rate-of-change of phase. Moreover, the calculated Doppler shift is related to the range rate. Doppler measurements are one of the most important radiometric data types used in orbit determination.

There are three types of Doppler measurement: one-way, two-way, and three-way. In all of these cases, the accumulating downlink carrier phase is measured and recorded.

With a one-way Doppler measurement, the spacecraft transmits a downlink carrier that is unrelated to any frequency source in the DSN and the downlink Doppler shift is determined. The frequency stability of the spacecraft oscillator used to generate the downlink carrier typically limits the performance of this Doppler measurement. Ultra-Stable Oscillators (USOs) are typically used for one-way Doppler measurement.

A two-way Doppler measurement employs an uplink from a Deep Space Station (DSS) and a downlink to that same station. The spacecraft's transponder tracks the arriving uplink carrier, whose frequency differs from that transmitted by the DSS by the uplink Doppler shift. The transponder produces a downlink carrier that is coherently related to the received uplink carrier. To be precise, the transmitted downlink carrier frequency equals the received uplink carrier frequency multiplied by a constant G, the transponding ratio. (The frequency multiplication is needed to achieve frequency separation between uplink and downlink carriers). The downlink carrier is received at the same DSS that transmitted the uplink carrier. The arriving downlink carrier experiences a two-way Doppler effect. The downlink carrier frequency is therefore different from that on the uplink because of the two-way Doppler effect and because of the transponding ratio.

Three-way Doppler measurement is similar to two-way measurement, except that the downlink carrier is received at a different DSS than that from which the uplink carrier was

transmitted. So in a three-way measurement there are three nodes present: transmitting DSS, spacecraft, and receiving DSS.

A two-way or three-way Doppler measurement originates at a DSS. The uplink carrier frequency is synthesized within the exciter from a highly stable frequency reference provided by the Frequency and Timing Subsystem (FTS). Since this reference is typically more stable than the spacecraft-borne oscillator, a two-way or three-way Doppler measurement is more accurate than a one-way measurement.

For two-way and three-way Doppler measurements, it is necessary to account for the transponding ratio G. It is usual to define two-way Doppler as the transmitted uplink carrier frequency minus the ratio of the received downlink carrier frequency to the factor G. With this definition, the two-way Doppler would be zero if there were no relative motion between the DSS and the spacecraft. For a receding spacecraft that is typical of deep space exploration, two-way Doppler is a positive quantity.

The instrumentation of a Doppler measurement within a DSS is shown in diagrammatic form for a one-way measurement in Figure 1 and for a two-way measurement in Figure 2. In all Doppler measurements, the downlink carrier from the Low-Noise Amplifier (LNA) passes to the Downlink Tracking and Telemetry Subsystem (DTT), which resides in part in the antenna and in part in the Signal Processing Center (SPC). The Radio-frequency to Intermediate-frequency Downconverter (RID), which is located at the antenna, synthesizes a local oscillator from a frequency reference supplied by the FTS and then heterodynes this local oscillator with the downlink carrier. The Intermediate-Frequency (IF) signal that results is sent to the Signal Processing Center (SPC).

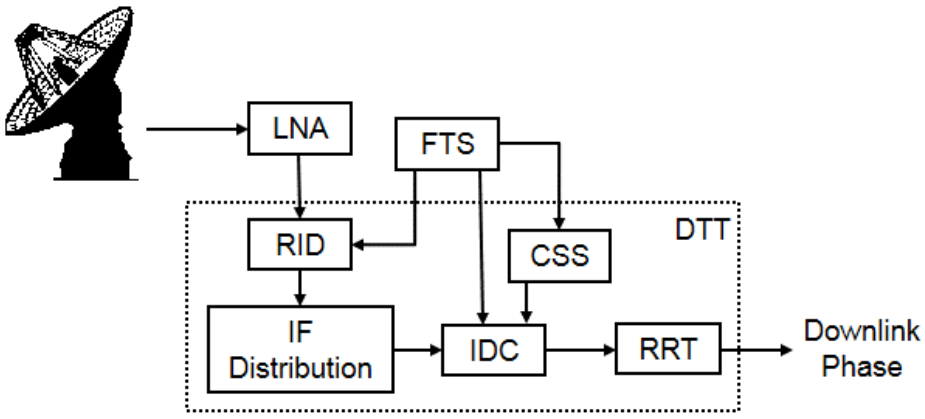

Figure 1. One-Way Doppler Measurement

In the SPC, the IF to Digital Converter (IDC) alters the frequency of the IF signal by a combination of up-conversion and down-conversion to a final analog frequency of approximately 200 MHz and then performs analog-to-digital conversion. The final analog stage of down-conversion uses a local oscillator supplied by the Channel-Select Synthesizer (CSS). The CSS is adjusted before the beginning of a pass to a frequency appropriate for the anticipated frequency range of the incoming downlink signal. During the pass, the frequency of the CSS

remains constant. The local oscillator frequencies of the CSS (and, indeed, of all local oscillators in the analog chain of down-conversion) are synthesized within the DTT from highly stable frequency references provided by the FTS. All analog stages of down-conversion are open-loop, and so the digital signal coming out of the IDC reflects the full Doppler shift.

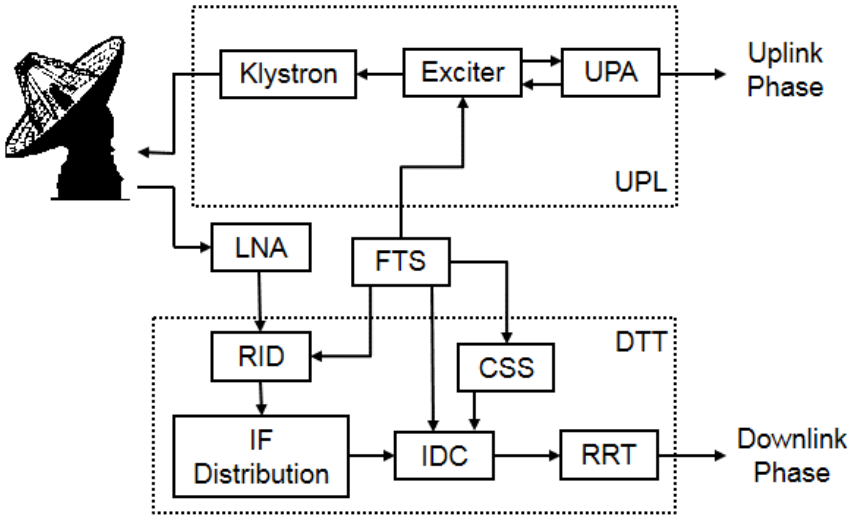

Figure 2. Two-Way Doppler Measurement

The Receiver, Ranging and Telemetry (RRT) processor accepts the signal from the IDC and extracts carrier phase with a digital phase-locked loop (Reference 1). The loop is configured to track the phase of a residual carrier, a suppressed carrier, or a QPSK (or Offset QPSK) signal. Since every analog local oscillator is held at constant frequency during a pass, the downlink carrier phase at sky frequency (that is, the phase that arrives at the DSS antenna) is easily computed from the local oscillator frequencies and the time-varying phase extracted by the digital phase-locked loop.

For a two-way or three-way Doppler measurement, the DSS exciter synthesizes the uplink carrier from a stable FTS frequency reference, as illustrated in Figure 2. The uplink carrier may be either constant or varied in accord with a tuning plan. In either case, the phase of the uplink carrier is recorded for use in the Doppler determination. The uplink phase counts are available from the Uplink Processor Assembly (UPA) at 1.0-second intervals.

The uplink and downlink carrier phase records must account for integer as well as fractional cycles. This is unlike many telecommunications applications where it is necessary to know the carrier phase only modulo one cycle. The reported data are uplink and downlink phase counts at sky frequency (but only downlink phase counts in the case of a one-way measurement). The downlink phase counts are available at 0.1-second intervals.

2.1 Carrier Loop Signal-to-Noise Ratio

The downlink carrier loop signal-to-noise ratio ρ_L must be known in order to calculate the Doppler measurement error and to calculate the variance of the phase error in the loop. The equation for ρ_L depends on the type of modulation on the downlink.

2.1.1 Residual Carrier

When the downlink carrier has a residual carrier and carrier synchronization is attained by tracking that residual carrier, ρ_L is

$$\rho_L = \frac{P_C}{N_0}\bigg|_{D/L} \cdot \frac{1}{B_L} \tag{1}$$

where

$P_C/N_0|_{D/L}$ = downlink residual-carrier power to noise spectral density ratio, Hz

B_L = one-sided, noise-equivalent bandwidth of the downlink carrier loop, Hz

When non-return-to-zero (NRZ) telemetry symbols directly modulate the carrier (in the absence of a subcarrier), there is an additional loss to the carrier loop signal-to-noise ratio. This loss is due to the presence of data sidebands overlaying the residual carrier in the frequency domain and therefore increasing the effective noise level for carrier synchronization. In this case, ρ_L must be calculated as (Reference 2)

$$\rho_L = \frac{P_C}{N_0}\bigg|_{D/L} \cdot \frac{1}{B_L} \cdot \frac{1}{1 + 2\,E_S/N_0} \tag{2}$$

where

E_S/N_0 = telemetry symbol energy to noise spectral density ratio

It is recommended that ρ_L meet the following constraint when the residual carrier is being tracked:

$$\rho_L \geq 10 \text{ dB}, \quad \text{residual carrier} \tag{3}$$

2.1.2 Suppressed-Carrier BPSK

A Costas loop is used to track a suppressed-carrier, binary phase-shift keyed (BPSK) carrier. For such a loop,

$$\rho_L = \frac{P_T}{N_0}\bigg|_{D/L} \cdot \frac{S_L}{B_L} \tag{4}$$

where

$P_T/N_0|_{D/L}$ = downlink total signal power to noise spectral density ratio, Hz

S_L = squaring loss of the Costas loop (Reference 3),

$$S_L = \frac{2\frac{E_S}{N_0}}{1 + 2\frac{E_S}{N_0}} \tag{5}$$

It is recommended that ρ_L meet the following constraint for suppressed-carrier BPSK tracking:

$$\rho_L \geq 17 \text{ dB}, \quad \text{suppressed-carrier BPSK} \tag{6}$$

This recommended minimum ρ_L is larger than for residual-carrier tracking because with a Costas loop there is the risk of half-cycle slips as well as full cycle slips.

2.1.3 QPSK and Offset QPSK

When tracking a quadriphase-shift keyed (QPSK) carrier or an Offset QPSK carrier, the loop signal to noise ratio is

$$\rho_L = \left.\frac{P_T}{N_0}\right|_{D/L} \cdot \frac{S_{LQ}}{B_L} \tag{7}$$

where (Reference 4)

$$S_{LQ} = \frac{1}{1 + \frac{9}{2R_d} + \frac{6}{{R_d}^2} + \frac{3}{2{R_d}^3}} \tag{8}$$

and (Reference 4)

$$R_d = 2\frac{E_S}{N_0} \tag{9}$$

E_S/N_0 is the ratio of the energy in one binary symbol to the noise spectral density. Since QPSK is more complicated than BPSK, it is worthwhile defining E_S/N_0 with an explicit formula:

$$\frac{E_S}{N_0} = \left.\frac{P_T}{N_0}\right|_{D/L} \cdot T_{S\,(\text{binary})} \tag{10}$$

where

$T_{S\,(\text{binary})}$ = period of the binary symbol, s

In the definition of $P_T/N_0|_{D/L}$ for QPSK, P_T is the *total* signal power; this includes the power in both phases of the carrier. The period $T_{S\,(\text{binary})}$ is the duration of a binary symbol at the input to the QPSK modulator (before the demultiplexer in the modulator) or, equivalently, at the output of the receiver's demodulator (after the multiplexer in the demodulator).

It is recommended that ρ_L meet the following constraint for QPSK and Offset QPSK:

$$\rho_L \geq 23, \text{dB} \quad \text{QPSK and Offset QPSK} \tag{11}$$

With a QPSK or Offset QPSK loop there is a risk of quarter-cycle slips and half-cycle slips as well as full cycle slips.

2.2 Doppler Measurement Error

The performance of one-way Doppler measurements and two-way (or three-way) coherent Doppler measurements is addressed here. Models are given for the important contributors to measurement error. More information about Doppler performance is available in References 5 and 6.

The error in Doppler measurement is characterized here as a standard deviation σ_V, having velocity units (such as $\mathrm{mm/s}$), or as a variance ${\sigma_V}^2$ ($\mathrm{mm^2/s^2}$). Models are given here for measurement error in the case of two-way (or three-way) coherent Doppler measurement and in the case of one-way Doppler measurement.

A Doppler measurement error can also be characterized as a standard deviation of frequency σ_f. This standard deviation and σ_V are related as follows:

$$\sigma_f = \begin{cases} \frac{f_C}{c}\sigma_V, & \text{one} - \text{way} \\ \frac{2f_C}{c}\sigma_V, & \text{two} - \text{way or three} - \text{way} \end{cases} \tag{12}$$

where

σ_V = standard deviation of range rate, same units as c

f_C = downlink carrier frequency

c = speed of electromagnetic waves in vacuum

σ_f = standard deviation of frequency, same units as f_C

The factor of 2 in Equation (12) for two-way and three-way measurements is present because σ_V represents the error in the rate-of-change of the (one-way) range and σ_f represents the error in the *total* Doppler shift, including uplink as well as downlink.

The error variance ${\sigma_V}^2$ for a Doppler measurement can be modeled as

$${\sigma_V}^2 = {\sigma_{VN}}^2 + {\sigma_{VF}}^2 + {\sigma_{VS}}^2 \tag{13}$$

where

${\sigma_V}^2$ = variance of range rate (square of σ_V)

${\sigma_{VN}}^2$ = contribution to ${\sigma_V}^2$ from white (thermal) noise

${\sigma_{VF}}^2$ = contribution to ${\sigma_V}^2$ from phase noise of frequency sources

${\sigma_{VS}}^2$ = contribution to ${\sigma_V}^2$ from (solar) phase scintillation

When telemetry data in an NRZ format directly modulate the carrier (that is, no subcarrier) and there is an imbalance in the data (that is, an unequal number of logical ones and zeros), a residual-carrier loop will experience an additional phase jitter. This phase jitter represents an additional error source for Doppler measurement, beyond those included in Equation (13). The standard deviation σ_{VI} of Doppler error due to telemetry data imbalance may be roughly modeled as follows:

$$\sigma_{VI} \cong \begin{cases} \dfrac{c \cdot \theta_t \cdot I_{\text{data}} \cdot B_L}{\sqrt{24} \cdot \pi \cdot f_C}, & \text{one} - \text{way} \\ \dfrac{c \cdot \theta_t \cdot I_{\text{data}} \cdot B_L}{2\sqrt{24} \cdot \pi \cdot f_C}, & \text{two} - \text{way or three} - \text{way} \end{cases} \tag{14}$$

where

σ_{VI} = standard deviation of Doppler error due to telemetry data imbalance, same units as c

θ_t = telemetry modulation index, rad

I_{data} = data imbalance, $0 \leq I_{\text{data}} \leq 0.5$

Data imbalance I_{data} is defined as follows. In a large set of $n_0 + n_1$ binary-valued telemetry symbols, if n_0 is the number of logical zeros and n_1 is the number of logical ones, $I_{\text{data}} = |n_0 - n_1|/(n_0 + n_1)$. The case $I_{\text{data}} = 0$ represents a perfect balance (and therefore $\sigma_{VI} = 0$). The case $I_{\text{data}} = 0.5$ represents the case where $n_0 = 3n_1$ (or vice versa), a highly imbalanced situation. It is possible, of course, for I_{data} to be larger than 0.5 (as large as 1, for which all symbols are identical); but the model of Equation (14) is only valid in the range $0 \leq I_{\text{data}} \leq 0.5$.

Pseudo randomization of the telemetry data can be employed in the transponder. When this is done, there is no significant data imbalance and the Doppler error σ_{VI} is 0.

2.2.1 One-Way Doppler Measurement Error

One-way Doppler measurement is subject to the following error sources: white noise at the receiver, phase noise originating in the frequency source on the spacecraft, and phase scintillation acquired by the downlink carrier in passing through the solar corona.

2.2.1.1 Downlink White (Thermal) Noise Contribution to $\sigma_V{}^2$, One-Way

For a one-way Doppler measurement, all of the white (thermal) noise originates on the downlink. The contribution ${\sigma_{VN}}^2$ is modeled as

$${\sigma_{VN}}^2 = 2 \cdot \left(\frac{c}{2\,\pi f_C T}\right)^2 \cdot \frac{1}{\rho_L}, \qquad \text{one-way} \tag{15}$$

where

T = integration time for Doppler measurement, s

The carrier loop signal-to-noise ratio ρ_L may be calculated from equations in Section 2.1.

2.2.1.2 Phase Noise Contribution to $\sigma_V{}^2$, One-Way

The frequency source of the downlink carrier introduces two kinds of error to a one-way Doppler measurement: an unknown bias and a random error. The bias is due to uncertainty in the transmitted frequency; this bias is not further discussed here. The random error is due to frequency instability of the frequency source. Frequency instability can be characterized either in terms of a fractional frequency deviation (the Allan deviation) or in terms of phase noise. If the phase noise of the source has been characterized, its contribution to $\sigma_V{}^2$ may be calculated as follows.

$$\sigma_{VF}{}^2 = \left(\frac{c}{\pi f_C T}\right)^2 \int_0^\infty S_{D/L}(f) \cdot \left|H_{D/L}(j2\pi f)\right|^2 \cdot \sin^2(\pi f T)\, df \tag{16}$$

where

$S_{D/L}(f)$ = one-sided power spectral density of downlink-carrier phase noise, rad^2/Hz

$H_{D/L}(j2\pi f)$ = frequency response of DTT receiver's carrier loop

The frequency response $H_{D/L}(j2\pi f)$ is related to the transfer function $H_{D/L}(s)$ of that loop by

$$H_{D/L}(j2\pi f) = H_{D/L}(s)\big|_{s=j2\pi f} \tag{17}$$

where s is the Laplace transform variable. The form of $H_{D/L}(s)$ depends on whether the DTT receiver is configured as a type 2 or type 3 loop. Appendix A provides equations for $H_{D/L}(s)$.

The product $S_{D/L}(f) \cdot \left|H_{D/L}(j2\pi f)\right|^2$ appearing in Equation (16) represents that portion of the (one-sided) power spectral density of the phase noise that lies in the passband of $H_{D/L}(j2\pi f)$. This shows that $\sigma_{VF}{}^2$ depends, in general, on the carrier-loop bandwidth B_L.

In order to keep the phase error of the carrier loop small, B_L is normally selected to be large enough to pass almost all of the (low-pass) power spectral density $S_{D/L}(f)$. In this typical scenario, $\sigma_{VF}{}^2$ becomes insensitive to the exact value of B_L. The following approximation is then possible:

$$\sigma_{VF} \cong c\, \sigma_y(T), \qquad \text{one-way} \tag{18}$$

where

$\sigma_y(T)$ = Allan deviation of the carrier's frequency source

Allan deviation is a dimensionless measure of the fractional frequency stability and is a function of the integration time T (Reference 7). When using Equation (18), the Allan deviation function should be evaluated at the Doppler measurement time T. When using the approximation of Equation (18), $\sigma_{VF}{}^2$ will, of course, be the square of the standard deviation σ_{VF}.

Equation (18) is an excellent approximation when the phase noise is predominantly white-in-frequency, for which $S_{D/L}(f) \propto 1/f^2$. Therefore, when the phase noise

is predominantly white-in-frequency and B_L is large enough that the carrier-loop phase error is small, then Equation (18) is an excellent estimate of σ_{VF} for one-way Doppler measurement.

In general, there is also a contribution to ${\sigma_{VF}}^2$ from phase noise in the local oscillators of the DTT receiving chain. This contribution may be calculated using an equation similar to Equation (16), with $S_{D/L}(f)$ replaced by the one-sided power spectral density of the local oscillator phase noise. This contribution will depend, in general, on B_L. However, if B_L is large enough that the carrier-loop phase error is small, then the contribution may be approximated as the square of the σ_{VF} calculated by Equation (18), where the local oscillator's Allan deviation is used. At the stations, the local oscillators are derived from the FTS, where the Allan deviation of the local oscillators is typically very small compared with that for the frequency source, onboard the spacecraft, of the downlink carrier (for non-coherent operation). The contribution of the local oscillators in one-way Doppler measurement at a station is therefore typically negligible by comparison. However, at a test facility where there is no FTS, the phase noise of the local oscillators might be a significant contributor to ${\sigma_{VF}}^2$.

It is expected that atomic clocks will in the future be employed on spacecraft; when this occurs, ${\sigma_{VF}}^2$ will be calculated as the sum of two components: one from the onboard atomic clock and one from the DTT receiving-chain local oscillators.

2.2.1.3 Phase Scintillation Contribution to ${\sigma_V}^2$, One-Way

A microwave carrier passing through the solar corona experiences phase scintillation, which introduces a random error to the Doppler measurement. The contribution ${\sigma_{VS}}^2$ of phase scintillation to Doppler measurement error depends on the Sun-Earth-probe angle, the carrier frequency f_C, and the integration time T. A coarse approximation for ${\sigma_{VS}}^2$ is:

$$ {\sigma_{VS}}^2 = \begin{cases} \dfrac{0.53\ C_{\text{band}}\ c^2}{{f_C}^2 T^{0.35} [\sin(\theta_{\text{SEP}})]^{2.45}}, & 0^\circ < \theta_{\text{SEP}} \le 90^\circ \\ \dfrac{0.53\ C_{\text{band}}\ c^2}{{f_C}^2 T^{0.35}}, & 90^\circ < \theta_{\text{SEP}} \le 180^\circ \end{cases} \tag{19} $$

where

θ_{SEP} = Sun-Earth-probe angle ($0^\circ < \theta_{\text{SEP}} \le 180^\circ$)

The standard deviation σ_{VS} (the square-root of the variance ${\sigma_{VS}}^2$) has the same dimensions as c. (The product $0.53\ C_{\text{band}}$ is not dimensionless; it has the same dimensions as ${f_C}^2 \cdot T^{0.35}$.)

The constant parameter C_{band} depends on the downlink band,

$$ C_{\text{band}} = \begin{cases} 2.6 \times 10^{-5}, & \text{S} - \text{down} \\ 1.9 \times 10^{-6}, & \text{X} - \text{down} \\ 1.3 \times 10^{-7}, & \text{Ka} - \text{down} \end{cases} \tag{20} $$

In Equation (19), ${\sigma_{VS}}^2$ is a continuous function of θ_{SEP} (when f_C and T are kept constant) for $0^\circ < \theta_{\text{SEP}} \le 180^\circ$.

Throughout this module, the designation "Ka" refers to the bands 34,200 to 34,700 MHz on the uplink and 31,800 to 32,300 MHz on the downlink. The DSN does not support radiometric measurements in the (downlink) band 25,500 to 27,000 MHz (K band).

The approximation of Equation (19) is based on the work reported in Reference 8. This model is valid when tracking binary phase-shift keyed telemetry with either a residual or suppressed carrier or when tracking a QPSK (or Offset QPSK) signal. This model is the recommended estimate for all Sun-Earth-probe angles, even though this model was originally based on data for Sun-Earth-probe angles between 5° and 27°. More recent measurements suggest that the estimate is more generally applicable. Reference 9, for example, validates the approximate model for Sun-Earth-probe angles less than 5°.

Figure 3 shows the standard deviation σ_{VS} (the square-root of the variance $\sigma_{VS}{}^2$) as a function of θ_{SEP} for one-way Doppler measurement with an S-band downlink. The vertical axis is in units of mm/s. Figure 4 shows σ_{VS} for an X-band downlink. Figure 5 shows σ_{VS} for a Ka-band downlink.

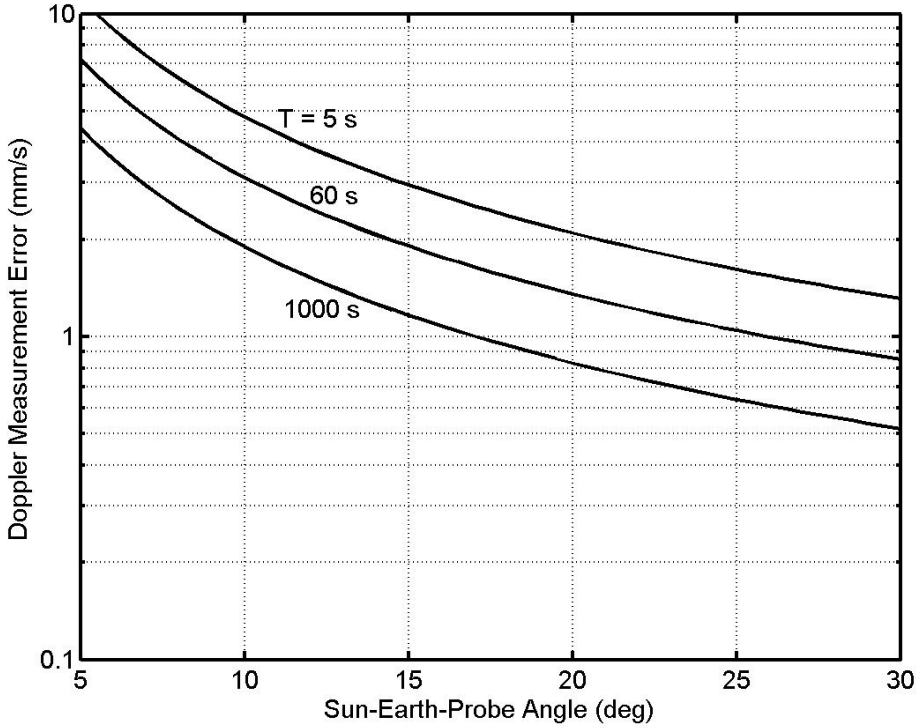

Figure 3. Doppler Measurement Error Due to Solar Phase Scintillation: S-Down

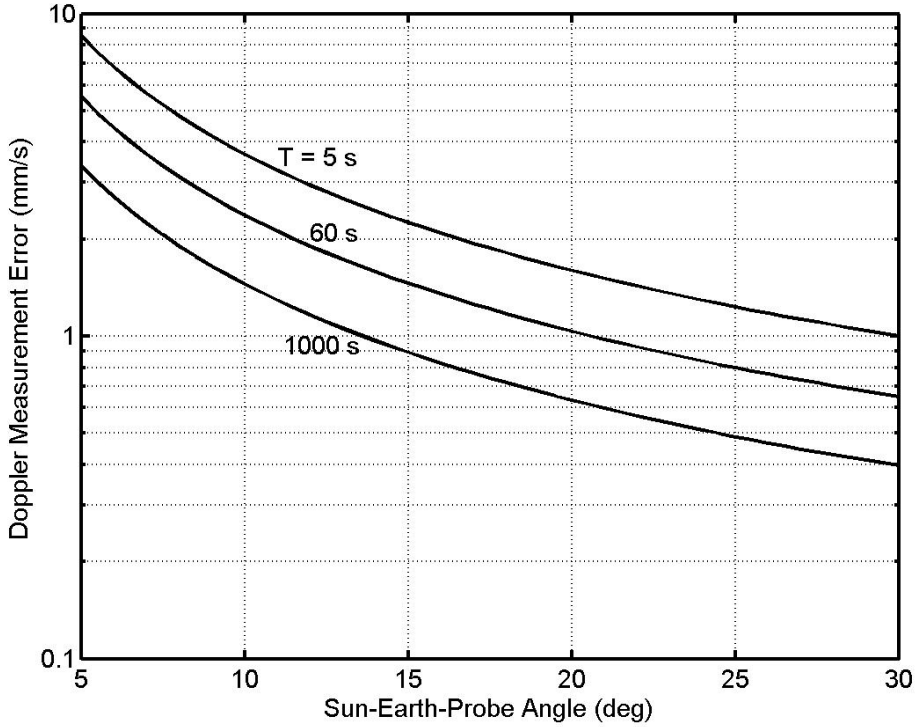

Figure 4: Doppler Measurement Error Due to Solar Phase Scintillation: X-Down

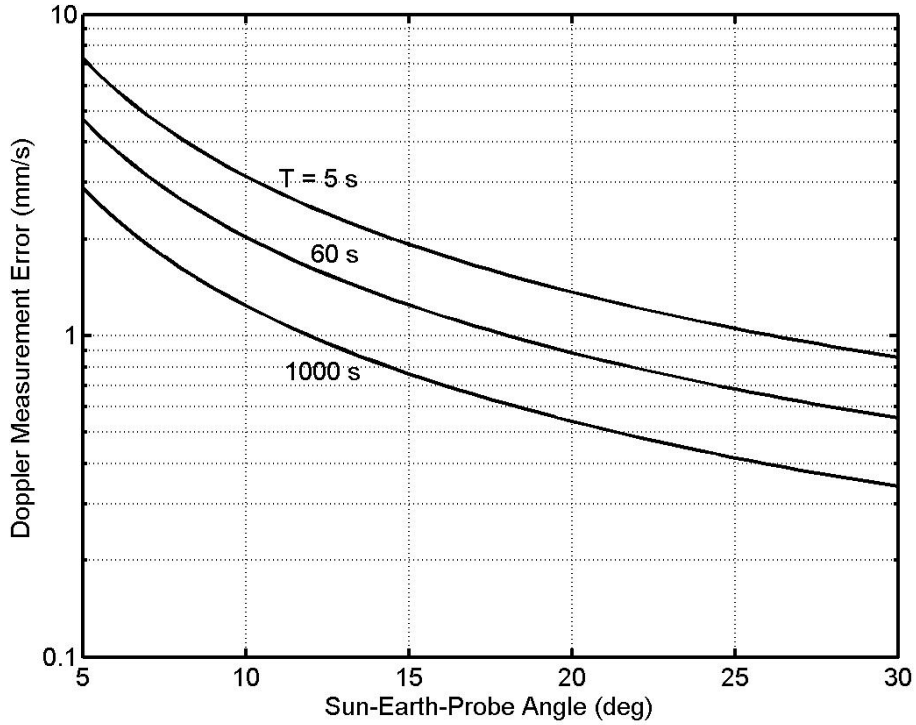

Figure 5. Doppler Measurement Error Due to Solar Phase Scintillation: Ka-Down

2.2.2 Two-Way and Three-Way Doppler Measurement Error

Two-way and three-way Doppler measurements are made with the spacecraft transponder in coherent mode. The most important error sources for coherent measurements are white noise on both the uplink and downlink and phase scintillation acquired by the uplink and downlink carriers in passing through the solar corona.

2.2.2.1 White (Thermal) Noise Contribution to $\sigma_V{}^2$, Two- and Three-Way

The white (thermal) noise contribution ${\sigma_{VN}}^2$ to two-way and three-way Doppler measurement error has two components:

$$ {\sigma_{VN}}^2 = {\sigma_{VNU}}^2 + {\sigma_{VND}}^2 \tag{21} $$

where

${\sigma_{VNU}}^2$ = contribution to ${\sigma_{VN}}^2$ from uplink white (thermal) noise

${\sigma_{VND}}^2$ = contribution to ${\sigma_{VN}}^2$ from downlink white (thermal) noise

The variance ${\sigma_{VNU}}^2$ accounts for white (thermal) noise that originates on the uplink, is tracked by the transponder's carrier loop, is transponded to the downlink band, and is tracked by the downlink receiver. For two- or three-way coherent Doppler measurement, the contribution ${\sigma_{VNU}}^2$ of uplink white noise is modeled as

$$ {\sigma_{VNU}}^2 = \frac{1}{2} \cdot \left(\frac{c}{2\,\pi f_C T} \right)^2 \cdot \frac{G^2}{\rho_{TR} \cdot B_{TR}} \int_0^\infty \left| H_{U/L}(j2\pi f) \right|^2 \cdot \left| H_{D/L}(j2\pi f) \right|^2 df \tag{22} $$

where

G = transponding ratio

ρ_{TR} = signal-to-noise ratio in transponder's carrier loop

B_{TR} = noise-equivalent bandwidth of the transponder's carrier loop, Hz

$H_{U/L}(j2\pi f)$ = frequency response of uplink (transponder) carrier loop

Here B_{TR} (Hz) is the noise-equivalent bandwidth of the transponder's carrier loop:

$$ B_{TR} = \int_0^\infty \left| H_{U/L}(j2\pi f) \right|^2 df \tag{23} $$

ρ_{TR} is the signal-to-noise ratio in the transponder's carrier loop with bandwidth B_{TR}. It can be calculated from equations similar to those given in Section 2.1 but using uplink parameters, instead of downlink parameters. For example, when the uplink is residual carrier, ρ_{TR} is calculated as the uplink residual-carrier power to noise spectral density ratio divided by B_{TR}. If the uplink were suppressed carrier and tracked by a Costas loop, ρ_{TR} would equal the uplink total signal power to noise spectral density ratio times a squaring loss divided by B_{TR}.

In order to evaluate Equation (22), it is also necessary to know the frequency response $H_{U/L}(j2\pi f)$ of the transponder's carrier loop. Fortunately, there is an approximation for ${\sigma_{VNU}}^2$ that requires only the bandwidth B_{TR} of the transponder's carrier loop. This approximation is

$$ {\sigma_{VNU}}^2 \cong \begin{cases} \frac{1}{2} \cdot \left(\frac{c}{2\,\pi f_C T}\right)^2 \cdot \frac{G^2}{\rho_{TR}} \cdot \frac{B_L}{B_{TR}}, & B_L < B_{TR} \\ \frac{1}{2} \cdot \left(\frac{c}{2\,\pi f_C T}\right)^2 \cdot \frac{G^2}{\rho_{TR}}, & B_L \geq B_{TR} \end{cases} \tag{24} $$

Equation (24) can be understood with the following heuristic argument. In the case $B_L < B_{TR}$, only a fraction B_L/B_{TR} of the uplink noise that is tracked by the transponder's carrier loop is also tracked by the DTT carrier loop; in this case, therefore, ${\sigma_{VNU}}^2$ is proportional to B_L/B_{TR}. In the case $B_L \geq B_{TR}$, all of the uplink noise that is tracked by the transponder's loop is also tracked by the DTT receiver's loop; therefore, B_L/B_{TR} is replaced by 1. When $B_L$and B_L are comparable (that is, when neither $B_L \gg B_{TR}$ nor $B_L \ll B_{TR}$), the best accuracy is obtained for ${\sigma_{VNU}}^2$ by using Equation (22).

The variance ${\sigma_{VND}}^2$ accounts for white (thermal) noise that originates on the downlink and is tracked by the DTT receiver. The contribution ${\sigma_{VND}}^2$ is modeled as

$$ {\sigma_{VND}}^2 = \frac{1}{2} \cdot \left(\frac{c}{2\,\pi f_C T}\right)^2 \cdot \frac{1}{\rho_L}, \qquad \text{two-way and three-way} \tag{25} $$

where ρ_L is the downlink carrier loop signal-to-noise ratio. Section 2.1 has equations for calculating ρ_L.

Equation (25) for two-way and three-way Doppler measurement is different from Equation (15) for one-way Doppler measurement. This difference is due to the fact that σ_V is the error in the determination of the range-of-change of a (one-way) range, so there must be a scaling by a factor of $1/2$ for a two-way (or three-way) measurement. This factor of $1/2$ also appears in Equation (12). For the variance ${\sigma_{VND}}^2$, the factor becomes $1/4$.

2.2.2.2 Phase Noise Contribution to ${\sigma_V}^2$, Two- and Three-Way

When making two- and three-way Doppler measurements at the stations (as opposed to the making of measurements entirely within a test facility), the contribution ${\sigma_{VF}}^2$ may be modeled as:

$$ {\sigma_{VF}}^2 = 2\left(\frac{c\,G}{2\pi f_C T}\right)^2 \int_0^\infty S_{U/L}(f) \cdot \left|H_{D/L}(j2\pi f)\right|^2 \cdot \sin^2(\pi f T)\, df, \tag{26} $$

two- and three-way coherent measurement at the stations

where

$S_{U/L}(f)$ = one-sided power spectral density of uplink-carrier phase noise, rad^2/Hz

Equation (26) accounts for both phase noise in the uplink frequency source and phase noise in the DTT receiving-chain local oscillators. For a three-way measurement, the

uplink source phase noise is independent of the local-oscillator phase noise. For a two-way coherent measurement in deep space, the round-trip signal delay is large enough that local-oscillator phase noise is uncorrelated with the delayed uplink source phase noise, even though both originate with a common FTS. The factor of 2 at the front of the right-hand side of Equation (26) is present because the total contribution ${\sigma_{VF}}^2$ is twice as large as a contribution from either the uplink-source phase noise alone or the local-oscillator phase noise alone.

The contribution ${\sigma_{VF}}^2$ depends on the DTT receiver carrier-loop bandwidth B_L, since the frequency response $H_{D/L}(j2\pi f)$ of this loop depends on B_L. In order to keep the phase error of the carrier loop small, B_L is normally selected to be large enough to pass almost all of the (low-pass) power spectral density $G^2 \cdot S_{U/L}(f)$. In this typical scenario, ${\sigma_{VF}}^2$ becomes insensitive to the exact value of B_L. The following approximation is then possible:

$$\sigma_{VF} \cong \frac{c\,\sigma_y(T)}{\sqrt{2}}, \qquad \text{two- and three-way} \qquad (27)$$

When using Equation (27), the Allan deviation function should be evaluated at the Doppler measurement time T. ${\sigma_{VF}}^2$ is the square of the standard deviation σ_{VF} given in Equation (27). When the phase noise is predominantly white-in-frequency, for which $S_{U/L}(f) \propto 1/f^2$, Equation (27) is an excellent approximation.

Equation (27) has a factor $1/\sqrt{2}$ that is absent in Equation (18). The two-way and three-way case accounts for both the uplink-source phase noise and the DTT receiver local-oscillator phase noise; this is a factor of 2 in ${\sigma_{VF}}^2$, or a factor of $\sqrt{2}$ in σ_{VF}. Moreover, σ_V is the error in the determination of the range-of-change of a (one-way) range, so there must be a scaling by a factor of $1/2$ for a two-way (or three-way) measurement.

Typically, ${\sigma_{VF}}^2$ is negligible for two-way and three-way Doppler measurement, owing to the excellent frequency stability of the frequency sources, which are derived at the stations from the FTS. It is possible, however, to cause ${\sigma_{VF}}^2$ to be significant during coherent operations by choosing a DTT receiver bandwidth B_L that is too small. However, if this is done, the DTT carrier loop will have a large phase error. In such a case, a poor ${\sigma_{VF}}^2$ might be the less concerning problem. Generally, for two-way or three-way coherent Doppler measurement with a spacecraft, a B_L of at least 1 Hz should ensure that ${\sigma_{VF}}^2$ will be small. However, the phase error in the carrier loop might still be a problem, depending on the rate-of-change and the acceleration of the downlink carrier's frequency.

When testing a transponder at the Development and Test Facility (DTF-21) or the Compatibility Test Trailer (CTT-22), the frequency stability of the uplink carrier and local oscillators is substantially poorer than at the stations. For a two-way Doppler measurement at DTF-21 or CTT-22, ${\sigma_{VF}}^2$ might be significant. For this scenario, ${\sigma_{VF}}^2$ can be modeled as:

$${\sigma_{VF}}^2 = \left(\frac{c\,G}{2\pi f_C T}\right)^2 \int_0^\infty S_{U/L}(f) \cdot \left|1 - H_{U/L}(j2\pi f)\right|^2 \cdot \left|H_{D/L}(j2\pi f)\right|^2 \cdot \sin^2(\pi f T)\, df, \qquad (28)$$

DTF-21 and CTT-22

Equation (28) reflects the fact that uplink-carrier phase noise will largely be canceled by phase noise in the local oscillators of the receiving chain but that this cancellation is imperfect when the transponder does not track all of the uplink-carrier phase noise. The term $S_{U/L}(f) \cdot \left|1 - H_{U/L}(j2\pi f)\right|^2$ represents that portion of the uplink-carrier phase noise that is not tracked by the transponder. When the transponder's carrier loop bandwidth is large enough that almost all of the uplink-carrier phase noise is tracked, the cancellation of downlink-carrier phase noise and receiving-chain local-oscillator phase noise will be nearly complete; and, under these circumstances, ${\sigma_{VF}}^2$ will be negligible.

2.2.2.3 Phase Scintillation Contribution to ${\sigma_V}^2$, Two- and Three-Way

The contribution ${\sigma_{VS}}^2$ of phase scintillation to Doppler measurement error may be approximated with Equation (19), which is repeated below for the reader's convenience.

$$ {\sigma_{VS}}^2 = \begin{cases} \dfrac{0.53\ C_{\text{band}}\ c^2}{{f_C}^2 T^{0.35} [\sin(\theta_{\text{SEP}})]^{2.45}}, & 0^\circ < \theta_{\text{SEP}} \leq 90^\circ \\ \dfrac{0.53\ C_{\text{band}}\ c^2}{{f_C}^2 T^{0.35}}, & 90^\circ < \theta_{\text{SEP}} \leq 180^\circ \end{cases} \tag{19} $$

As before, θ_{SEP} is the Sun-Earth probe angle ($0^\circ < \theta_{\text{SEP}} \leq 180^\circ$), T is the measurement integration time, f_C is the downlink carrier frequency, and c is the speed of electromagnetic waves in vacuum. The standard deviation σ_{VS} (the square-root of the variance ${\sigma_{VS}}^2$) has the same dimensions as c. (The product $0.53\ C_{\text{band}}$ is not dimensionless; it has the same dimensions as ${f_C}^2 \cdot T^{0.35}$.)

Equation (19) is applicable to two-way and three-way Doppler measurements, as well as one-way measurements. The parameter C_{band} is different for two-way (and three-way) Doppler measurement than for one-way Doppler measurement. The parameter C_{band} depends on the uplink/downlink band pairing,

$$ C_{\text{band}} = \begin{cases} 6.1 \times 10^{-5}, & \text{S} - \text{up/S} - \text{down} \\ 4.8 \times 10^{-4}, & \text{S} - \text{up/X} - \text{down} \\ 2.6 \times 10^{-5}, & \text{X} - \text{up/S} - \text{down} \\ 5.5 \times 10^{-6}, & \text{X} - \text{up/X} - \text{down} \\ 5.2 \times 10^{-5}, & \text{X} - \text{up/Ka} - \text{down} \\ 1.9 \times 10^{-6}, & \text{Ka} - \text{up/X} - \text{down} \\ 2.3 \times 10^{-7}, & \text{Ka} - \text{up/Ka} - \text{down} \end{cases} \tag{29} $$

Throughout this module, the designation "Ka" refers to the bands 34,200 to 34,700 MHz on the uplink and 31,800 to 32,300 MHz on the downlink. The DSN does not support radiometric measurements in the (downlink) band 25,500 to 27,000 MHz (K band).

The approximation of Equation (19) is based on the work reported in Reference 8. This model is valid when tracking binary phase-shift keyed telemetry with either a residual or suppressed carrier or when tracking a QPSK (or Offset QPSK) signal. This model is the recommended estimate for all Sun-Earth-probe angles, even though this model was originally based on data for Sun-Earth-probe angles between 5° and 27°. More recent measurements

suggest that the estimate is more generally applicable. Reference 9, for example, validates the approximate model for Sun-Earth-probe angles less than 5°.

Figure 6 shows the standard deviation σ_{VS} (the square-root of the variance $\sigma_{VS}{}^2$) as a function of Sun-Earth-probe angle for two-way or three-way Doppler measurement with an S-band uplink and an S-band downlink. The vertical axis is in units of mm/s. The three curves in that figure correspond to measurement integration times of 5, 60, and 1000 seconds. Figure 7 shows σ_{VS} for an S-band uplink and an X-band downlink. Figure 8 shows σ_{VS} for an X-band uplink and an S-band downlink. Figure 9 shows σ_{VS} for an X-band uplink and an X-band downlink. Figure 10 shows σ_{VS} for an X-band uplink and a Ka-band downlink. Figure 11 shows σ_{VS} for a Ka-band uplink and an X-band downlink. Figure 12 shows σ_{VS} for a Ka-band uplink and a Ka-band downlink. In comparing these figures, it should be noted that the vertical scale is not the same for all of these figures.

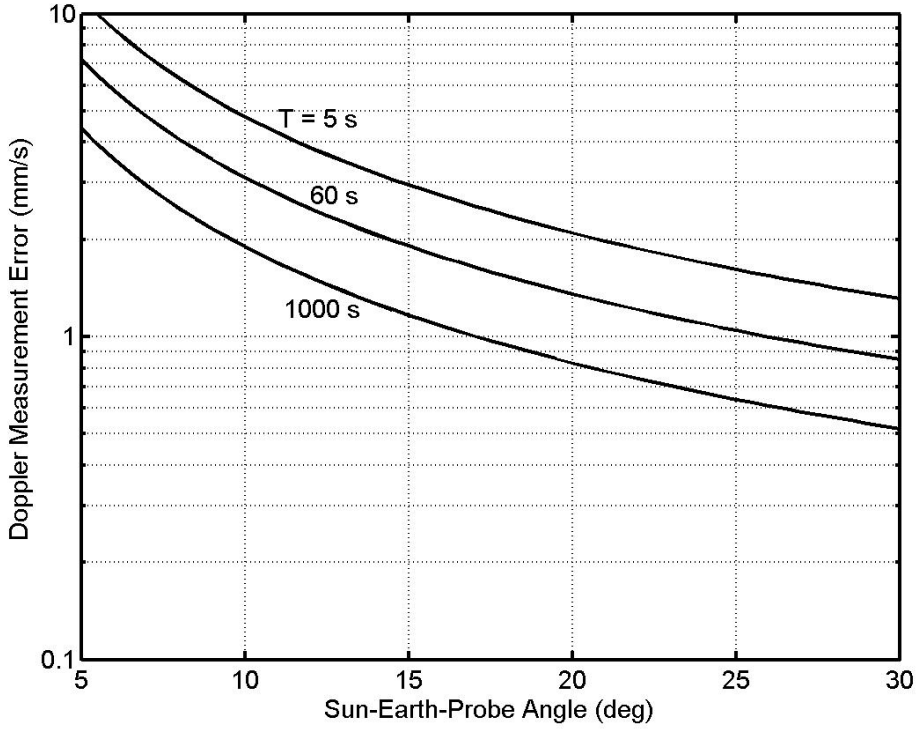

Figure 6. Doppler Measurement Error Due to Solar Phase Scintillation: S-Up/S-Down

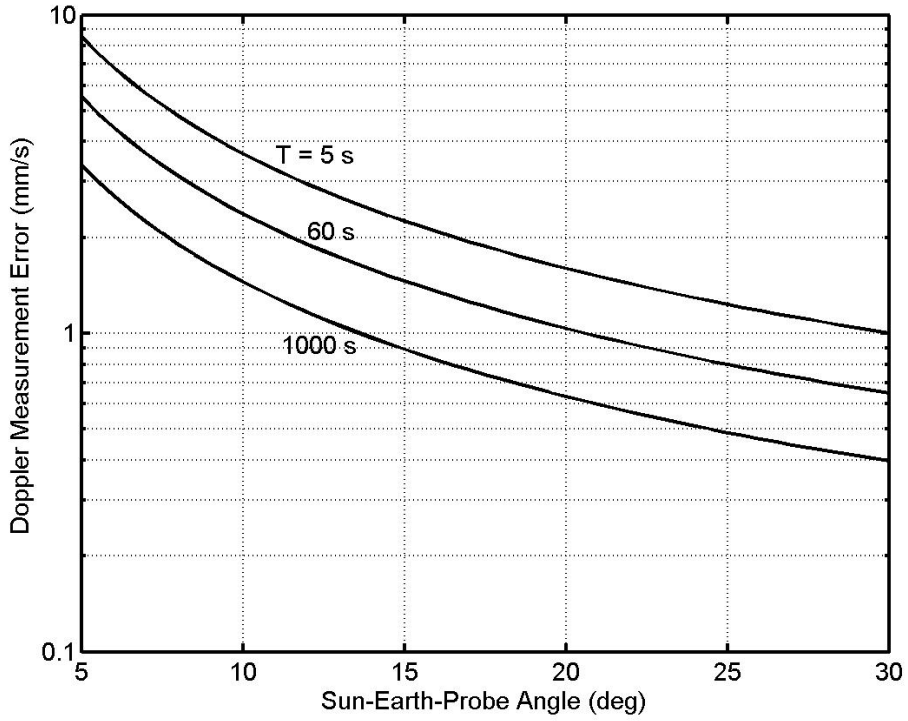

Figure 7. Doppler Measurement Error Due to Solar Phase Scintillation: S-Up/X-Down

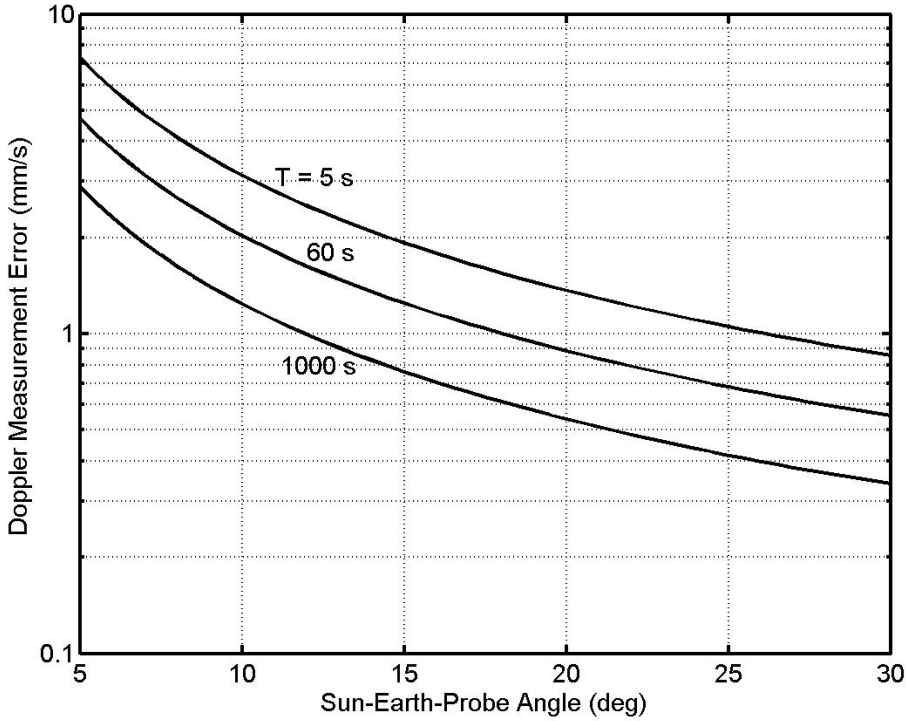

Figure 8. Doppler Measurement Error Due to Solar Phase Scintillation: X-Up/S-Down

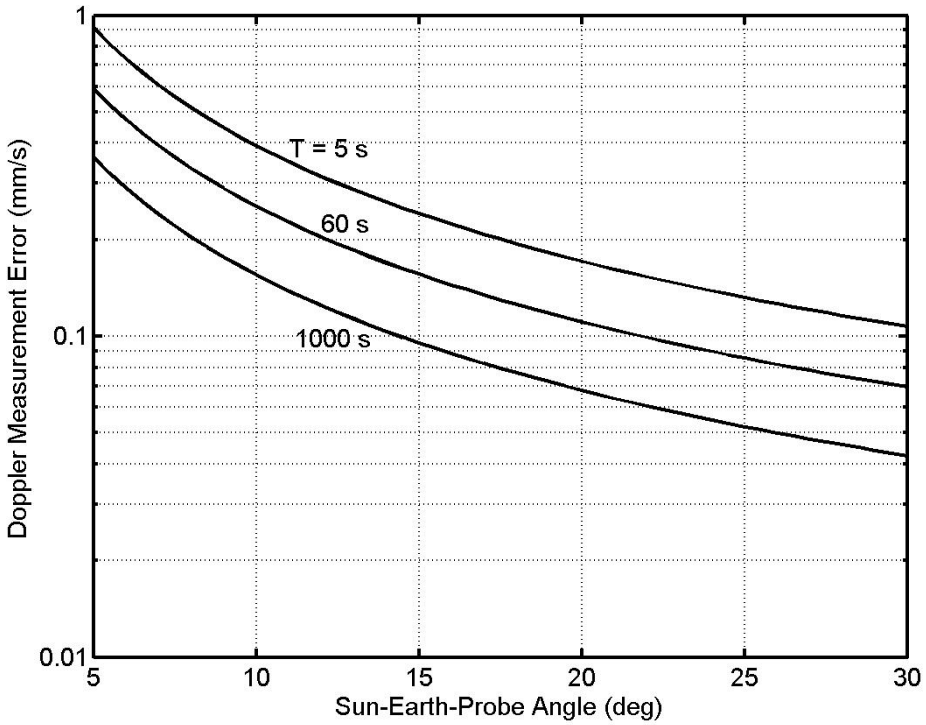

Figure 9. Doppler Measurement Error Due to Solar Phase Scintillation: X-Up/X-Down

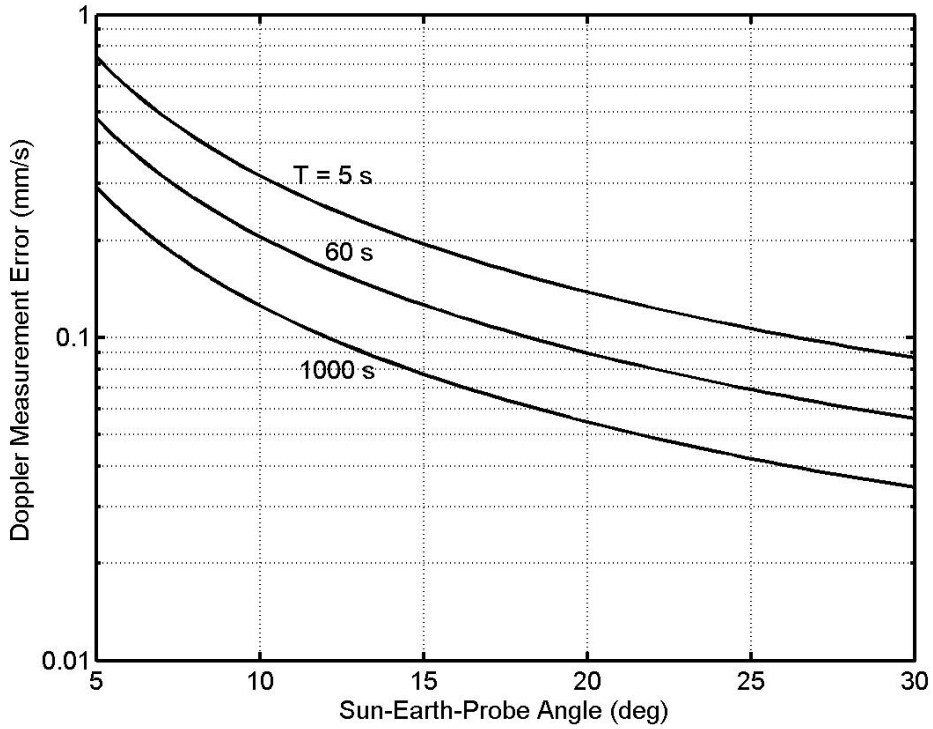

Figure 10. Doppler Measurement Error Due to Solar Phase Scintillation: X-Up/Ka-Down

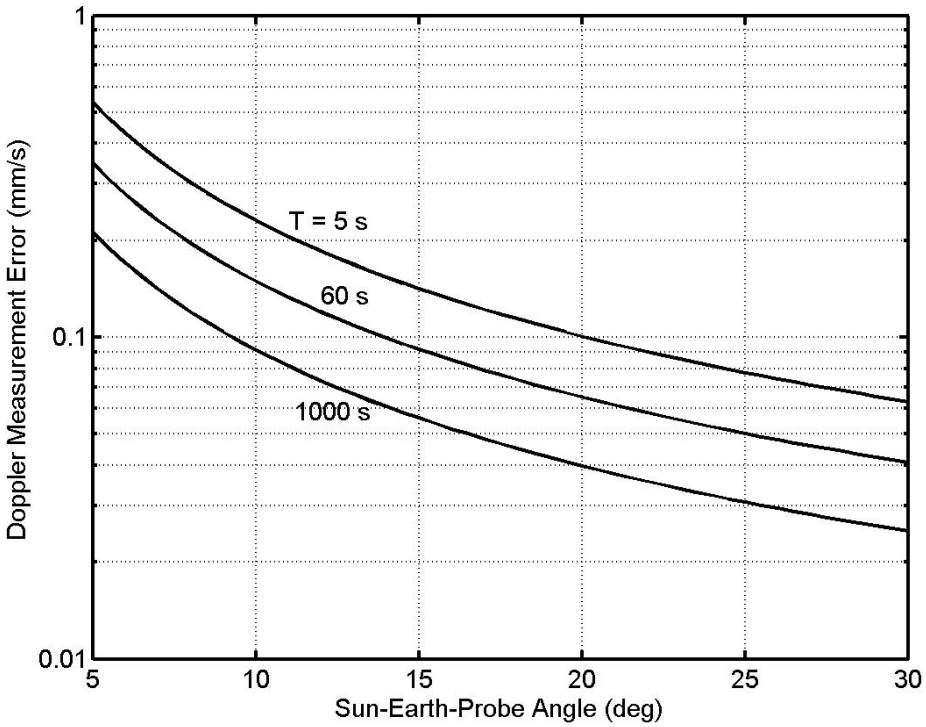

Figure 11. Doppler Measurement Error Due to Solar Phase Scintillation: Ka-Up/X-Down

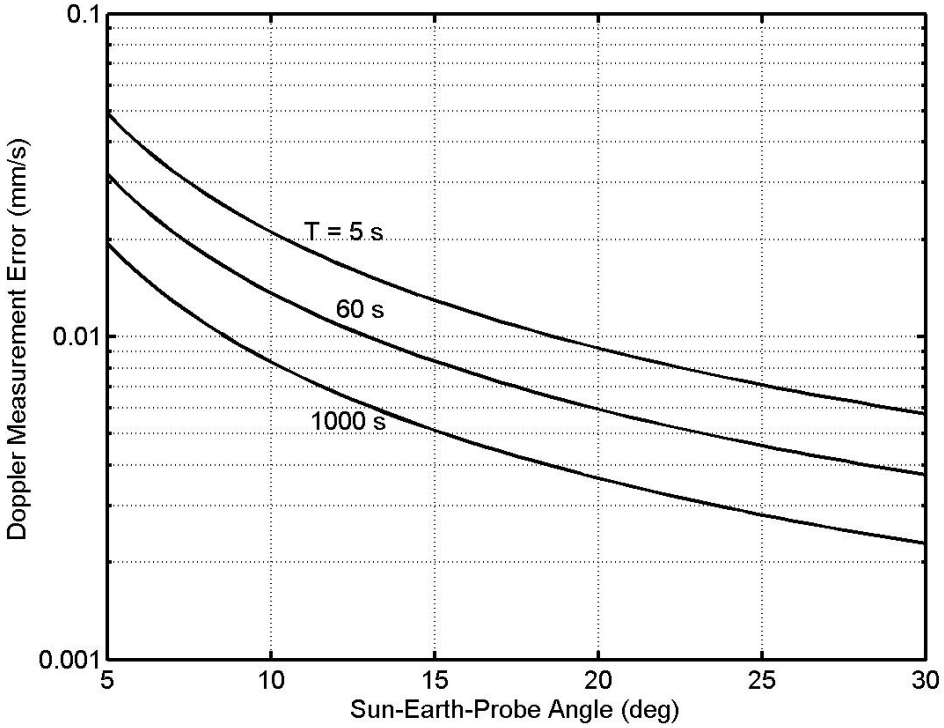

Figure 12. Doppler Measurement Error Due to Solar Phase Scintillations: Ka-Up/Ka-Down

2.3 Carrier Tracking

The DTT receiver can be configured to track phase-shift keyed telemetry with a residual carrier or a suppressed carrier or to track a QPSK or Offset QPSK signal. In order to achieve good telemetry performance and good Doppler measurement performance, it is important to characterize the phase error in the carrier loop.

2.3.1 Carrier Power Measurement

When the downlink is residual-carrier, an estimate of the downlink residual-carrier power P_C is available. When the downlink is suppressed-carrier, an estimate of the total downlink power P_T is available. This is done by first estimating $P_C/N_0|_{D/L}$ (with a modified version of the algorithm described in Reference 10) or $P_T/N_0|_{D/L}$ (with the split-symbol moments algorithm described in Reference 11). An estimate of the noise spectral density N_0 comes from continual measurements made by a noise-adding radiometer. This information is used to compute absolute power P_C or P_T. The results are reported once per second.

2.3.2 Carrier Loop Bandwidth

The one-sided, noise-equivalent, carrier loop bandwidth of the DTT receiver is denoted B_L. The user may choose to change B_L during a tracking pass, and this can be implemented without losing phase-lock, assuming the change is not too large. There are limits on the carrier loop bandwidth. For the DTT receiver, B_L can be no larger than 200 Hz. The lower limit on B_L is determined by the phase noise on the downlink. In addition, when operating in the suppressed-carrier mode, B_L is subject to the following constraint.

$$B_L \leq \frac{R_{SYM}}{20}, \text{ suppressed carrier} \tag{30}$$

where

R_{SYM} = telemetry symbol rate

In general, the value selected for B_L should be small in order to maximize the carrier loop signal-to-noise ratio. On the other hand, B_L must be large enough that neither of the following variables becomes too large: the static phase error due to Doppler dynamics and the contribution to carrier loop phase error variance from phase noise on the downlink. The best B_L to select will depend on circumstances. Often, it will be possible to select a B_L of about 1 Hz. A larger value for B_L is necessary when there is significant uncertainty in the downlink Doppler dynamics, when the downlink is one-way (or two-way non-coherent) and originates with a less stable frequency source, or when the Sun-Earth-probe angle is small (so that solar phase scintillations are present on the downlink).

When tracking a spinning spacecraft, it may be necessary to set the carrier loop bandwidth to a value that is somewhat larger than would otherwise be needed. The loop bandwidth must be large enough to track out the variation due to the spin. Also, the coherent AGC in the receiver must track out the amplitude variations.

The user may select either a type 2 or type 3 carrier loop. Both loop types are perfect, meaning that the loop filter implements a true accumulation.

2.3.3 Static Phase Error in the Carrier Loop

The carrier loop, with either a type 2 or type 3 loop, has a very large tracking range; even a Doppler offset of several megahertz can be tracked. With a finite Doppler rate, however, there will be a static phase error in a type 2 loop.

Table 1 shows the static phase error in the carrier loop that results from various Doppler dynamics for several different loops. These equations are based on the work reported in Reference 12. The Doppler dynamics are here defined by the parameters α and β.

α = Doppler Rate, Hz/s

β = Doppler Acceleration, $\mathrm{Hz/s^2}$

In the presence of a persistent Doppler acceleration, a type 2 loop will periodically slip cycles. The equations of Table 1 are valid when tracking binary phase-shift keyed telemetry with either a residual or suppressed carrier or when tracking a QPSK or Offset QPSK signal. These equations are exactly the same as those appearing in Module 207.

Table 1. Static Phase Error (rad)

Loop	Constant Range Rate (Constant Doppler Offset)	Constant Derivative of Range Rate (Constant Doppler Rate)	Constant Second Derivative of Range Rate (Constant Doppler Acceleration)
type 2, standard underdamped	0	$\frac{9\pi\alpha}{16{B_L}^2}$	$\left(\frac{9\pi\beta}{16{B_L}^2}\right)t - \frac{27\pi\beta}{64{B_L}^3}$
type 2, supercritically damped	0	$\frac{25\pi\alpha}{32{B_L}^2}$	$\left(\frac{25\pi\beta}{32{B_L}^2}\right)t - \frac{125\pi\beta}{128{B_L}^3}$
type 3, standard underdamped	0	0	$\frac{12167\pi\beta}{8000{B_L}^3}$
type 3, supercritically damped	0	0	$\frac{35937\pi\beta}{16384{B_L}^3}$

2.3.4 Carrier Phase Error Variance

In order to ensure a strong phase lock, the phase error variance in the downlink carrier loop should be small. If this variance grows too large, both telemetry detection and Doppler measurement may suffer. This is, however, a second-order effect. For a baseline assessment of Doppler measurement error, the equations of Section 2.2 should be used.

In general, the carrier phase error variance ${\sigma_\phi}^2$ may be modeled as

$$\sigma_\phi{}^2 = \sigma_{\phi N}{}^2 + \sigma_{\phi F}{}^2 + \sigma_{\phi S}{}^2 \tag{31}$$

where

$\sigma_\phi{}^2$ = carrier phase error variance, rad^2

$\sigma_{\phi N}{}^2$ = contribution to $\sigma_\phi{}^2$ from white (thermal) noise, rad^2

$\sigma_{\phi F}{}^2$ = contribution to $\sigma_\phi{}^2$ from phase noise of frequency sources, rad^2

$\sigma_{\phi S}{}^2$ = contribution to $\sigma_\phi{}^2$ from (solar) phase scintillation, rad^2

Equation (31) does *not* characterize Doppler measurement error; rather it characterizes the variance of the phase error in the DTT receiver's carrier loop. For characterizing the Doppler measurement error, Equation (13) should be used. The loop phase error is, however, relevant because if the phase error is large it has a second-order effect on the Doppler measurement.

The models for $\sigma_{\phi N}{}^2$, $\sigma_{\phi F}{}^2$, and $\sigma_{\phi S}{}^2$ depend on whether the transponder is in coherent or non-coherent mode.

It is recommended that the variance $\sigma_\phi{}^2$ of the downlink receiver's carrier loop not exceed the following limits:

$$\sigma_\phi{}^2 \leq \begin{cases} 0.1 \text{ rad}^2, & \text{residual carrier} \\ 0.02 \text{ rad}^2, & \text{suppressed carrier BPSK} \\ 0.005 \text{ rad}^2, & \text{QPSK or Offset QPSK} \end{cases} \tag{32}$$

The limits of Equation (32) are consistent with the limits on ρ_L given in Equations (3), (6) and (11) for the case where the only significant contributor to $\sigma_\phi{}^2$ is downlink thermal noise.

The recommended maximum variance $\sigma_\phi{}^2$ of Equation (32) is intended for the case of zero static phase error. If there is a significant static phase error, $\sigma_\phi{}^2$ should be smaller than the maximum given by Equation (32). As a rough guide, the maximum value of $\sigma_\phi{}^2$ (rad^2) in the presence of a static phase error ϕ_{SPE} (rad) should be less than the suggested maximum of Equation (32) by $\phi_{\text{SPE}}{}^2$.

2.3.4.1 Non-Coherent Operation

For non-coherent operation (such as one-way), the important contributors to $\sigma_\phi{}^2$ are: white noise at the receiver, phase noise originating in the frequency source on the spacecraft, and phase scintillation acquired by the downlink carrier in passing through the solar corona.

2.3.4.1.1 Downlink White (Thermal) Noise Contribution to $\sigma_\phi{}^2$, Non-Coherent

The variance $\sigma_{\phi N}{}^2$ accounts for white (thermal) noise.

$$\sigma_{\phi N}{}^2 = \frac{1}{\rho_L}, \qquad \text{non-coherent} \tag{33}$$

where ρ_L is the downlink carrier loop signal-to-noise ratio. Section 2.1 has equations for calculating ρ_L.

2.3.4.1.2 Phase Noise Contribution to $\sigma_\phi{}^2$, Non-Coherent

The frequency source for the (non-coherent) downlink carrier has inherent phase noise. When this phase noise is characterized by the one-sided power spectral density $S_{D/L}(f)$, having units rad^2/Hz, ${\sigma_{\phi F}}^2$ is given by

$$ {\sigma_{\phi F}}^2 = \int_0^\infty S_{D/L}(f) \cdot \left|1 - H_{D/L}(j2\pi f)\right|^2 df \tag{34} $$

$H_{D/L}(j2\pi f)$ is the frequency response of the downlink carrier loop and is given in Appendix A for type 2 and type 3 DTT carrier loops. This transfer function depends on the noise-equivalent loop bandwidth B_L.

The term $S_{D/L}(f) \cdot \left|1 - H_{D/L}(j2\pi f)\right|^2$ represents that portion of the downlink-carrier phase noise that is not tracked by the DTT carrier loop. Without evaluating the integral of Equation (34), it is possible to say that ${\sigma_{\phi F}}^2$ decreases with increasing B_L. When B_L is large enough that almost all of the downlink-carrier phase noise is tracked, ${\sigma_{\phi F}}^2$ will be negligible.

In general, there is also a contribution to ${\sigma_{\phi F}}^2$ from phase noise in the local oscillators of the DTT receiving chain. This contribution may be calculated using an equation similar to Equation (34), with $S_{D/L}(f)$ replaced by the one-sided power spectral density of the local oscillator phase noise. Since the local oscillators are derived from the FTS, this contribution has typically been very small compared with that for the frequency source, onboard the spacecraft, of the downlink carrier (for non-coherent operation). It is expected that atomic clocks will in the future be employed on spacecraft; when this occurs, ${\sigma_{\phi F}}^2$ will be calculated as the sum of two components: one from the onboard atomic clock and one from the DTT receiving-chain local oscillators.

2.3.4.1.3 Phase Scintillation Contribution to $\sigma_\phi{}^2$, Non-Coherent

The contribution ${\sigma_{\phi S}}^2$ may be approximated by

$$ {\sigma_{\phi S}}^2 = \begin{cases} \dfrac{C_{\text{band}} \cdot C_{\text{loop}}}{[\sin(\theta_{\text{SEP}})]^{2.45} \cdot {B_L}^{1.65}}, & 0^\circ < \theta_{\text{SEP}} \le 90^\circ \\ \dfrac{C_{\text{band}} \cdot C_{\text{loop}}}{{B_L}^{1.65}}, & 90^\circ < \theta_{\text{SEP}} \le 180^\circ \end{cases} \tag{35} $$

θ_{SEP} is the Sun-Earth-probe angle ($0^\circ < \theta_{\text{SEP}} \le 180^\circ$). ${\sigma_{\phi S}}^2$ has the dimensions rad^2. (The product $C_{\text{band}} \cdot C_{\text{loop}}$ has the same dimensions as ${B_L}^{1.65}$.) The parameter C_{band} is constant for any given band and is given by Equation (20), which is repeated below for the reader's convenience.

$$C_{\text{band}} = \begin{cases} 2.6 \times 10^{-5}, & \text{S} - \text{down} \\ 1.9 \times 10^{-6}, & \text{X} - \text{down} \\ 1.3 \times 10^{-7}, & \text{Ka} - \text{down} \end{cases} \tag{20}$$

The parameter C_{loop} is constant for a given loop.

$$C_{\text{loop}} = \begin{cases} 5.9, & \text{standard underdamped type 2 loop} \\ 5.0, & \text{supercritically damped type 2 loop} \\ 8.2, & \text{standard underdamped type 3 loop} \\ 6.7, & \text{supercritically damped type 3 loop} \end{cases} \tag{36}$$

Equation (35) indicates that ${\sigma_{\phi S}}^2$ increases as θ_{SEP} decreases and as B_L decreases. Equation (20) indicates that ${\sigma_{\phi S}}^2$ increases with decreasing downlink carrier frequency.

2.3.4.2 Coherent Operation

The most important contributors to the carrier phase error variance ${\sigma_{\phi}}^2$ for coherent operation are white noise on both the uplink and downlink and phase scintillation acquired by the uplink and downlink carriers in passing through the solar corona.

2.3.4.2.1 White (Thermal) Noise Contribution to ${\sigma_{\phi}}^2$, Coherent

The white (thermal) noise contribution ${\sigma_{\phi N}}^2$ to carrier phase error variance ${\sigma_{\phi}}^2$ has two components:

$${\sigma_{\phi N}}^2 = {\sigma_{\phi NU}}^2 + {\sigma_{\phi ND}}^2 \tag{37}$$

where

${\sigma_{\phi NU}}^2$ = contribution to ${\sigma_{\phi N}}^2$ from uplink white (thermal) noise, rad^2

${\sigma_{\phi ND}}^2$ = contribution to ${\sigma_{\phi N}}^2$ from downlink white (thermal) noise, rad^2

For coherent operation, the contribution ${\sigma_{\phi NU}}^2$ of uplink white noise is modeled as

$${\sigma_{\phi NU}}^2 = \frac{G^2}{\rho_{TR} \cdot B_{TR}} \int_0^{\infty} \left|H_{U/L}(j2\pi f)\right|^2 \cdot \left|1 - H_{D/L}(j2\pi f)\right|^2 df \tag{38}$$

where

B_{TR} = transponder's carrier-loop bandwidth, Hz

Equation (38) accounts for noise that originates on the uplink, is tracked by the transponder's carrier loop, is transponded to the downlink band, and is *not* tracked by the DTT carrier loop. ${\sigma_{\phi NU}}^2$ generally increases as the DTT carrier-loop bandwidth B_L decreases. In the case where B_L is much smaller than the transponder's carrier-loop bandwidth B_{TR}, the following approximation is accurate:

$$\sigma_{\phi NU}{}^2 \cong \frac{G^2}{\rho_{TR}}, \qquad B_L \ll B_{TR} \tag{39}$$

Equation (39) is as an upper bound on $\sigma_{\phi NU}{}^2$. This upper bound is accurate when $B_L \ll B_{TR}$.

In general, when B_L is comparable with B_{TR} or larger than B_{TR}, the integral of Equation (38) must be evaluated in order to obtain an accurate value for $\sigma_{\phi NU}{}^2$. Both terms $\left|H_{U/L}(j2\pi f)\right|^2$ and $\left|1 - H_{D/L}(j2\pi f)\right|^2$, considered as functions of Fourier frequency, have relatively large transition bands. This is because they represent filters that are only of second or third order. These two functions of Fourier frequency are plotted in Figure 13 for a case where $B_L = B_{TR}$. In this case, there is considerable overlap between the functions. So it would clearly be a mistake for the case $B_L = B_{TR}$ to assume that $\sigma_{\phi NU}{}^2$ is zero (based on the simple notion that $\sigma_{\phi NU}{}^2$ represents uplink white noise that lies simultaneously inside B_{TR} and outside $B_L = B_{TR}$).

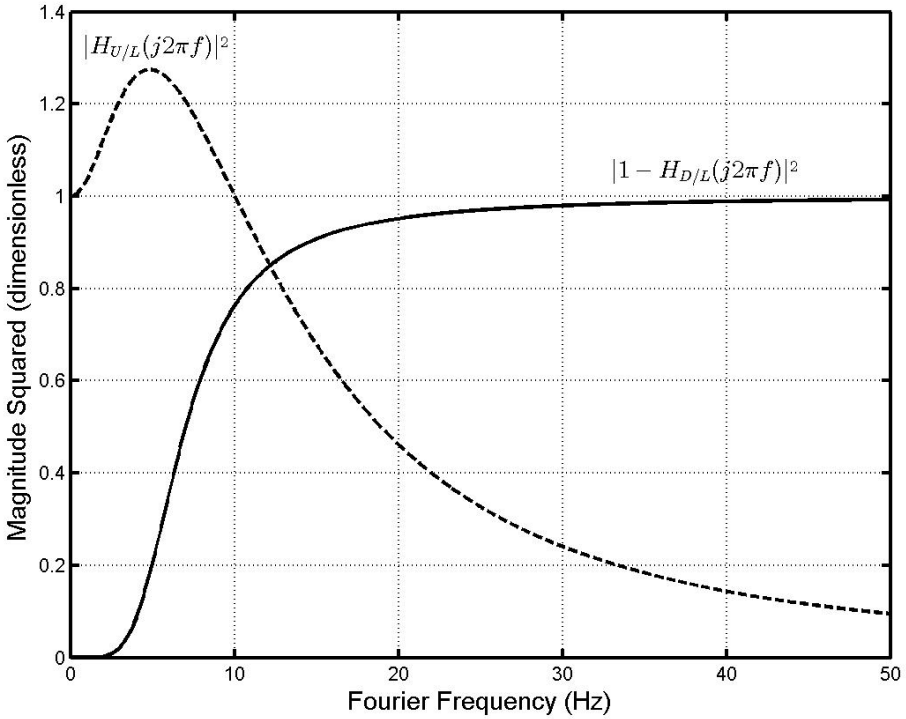

Figure 13. Terms Relating U/L White Noise to D/L Carrier Phase-Error Variance

The variance $\sigma_{\phi ND}{}^2$ (rad^2) accounts for white (thermal) noise that originates on the downlink.

$$\sigma_{\phi ND}{}^2 = \frac{1}{\rho_L} \tag{40}$$

where ρ_L is the downlink carrier loop signal-to-noise ratio. Section 2.1 has equations for calculating ρ_L.

2.3.4.2.2 Phase Noise Contribution to $\sigma_\phi{}^2$, Coherent

For coherent operations at the stations (but not at a test facility), the contribution $\sigma_{\phi F}{}^2$ may be modeled as:

$$\sigma_{\phi F}{}^2 = 2\,G^2 \int_0^\infty S_{U/L}(f) \cdot \left|1 - H_{D/L}(j2\pi f)\right|^2 df, \tag{41}$$

coherent operation at the stations

Equation (41) accounts for both phase noise in the uplink frequency source and phase noise in the DTT receiving-chain local oscillators. For a three-way measurement, the uplink source phase noise is independent of the local-oscillator phase noise. For a two-way coherent measurement in deep space, the round-trip signal delay is large enough that local-oscillator phase noise is uncorrelated with the delayed uplink source phase noise, even though both originate with a common FTS. The factor of 2 at the front of the right-hand side of Equation (41) is present because the total contribution $\sigma_{VF}{}^2$ is twice as large as a contribution from either the uplink-source phase noise alone or the local-oscillator phase noise alone.

The term $G^2 \cdot S_{U/L}(f) \cdot \left|1 - H_{D/L}(j2\pi f)\right|^2$ represents that portion of the downlink-carrier phase noise that is not tracked by the DTT carrier loop. Without evaluating the integral of Equation (41), it is possible to say that $\sigma_{\phi F}{}^2$ decreases with increasing B_L. When B_L is large enough that almost all of the downlink-carrier phase noise is tracked, $\sigma_{\phi F}{}^2$ will be negligible. A DTT carrier-loop bandwidth B_L of at least 1 Hz is adequate to ensure that $\sigma_{\phi F}{}^2$ is small while tracking a coherent downlink carrier. Of course, the rate-of-change and the acceleration of the downlink carrier's frequency causes a static phase error; therefore, B_L must be chosen large enough to ensure that this static phase error is not a problem.

At DTF-21 and CTT-22 the frequency stability of the uplink carrier and local oscillators is substantially poorer than at the stations; so, for coherent operation, $\sigma_{\phi F}{}^2$ might be significant. For this scenario, $\sigma_{\phi F}{}^2$ can be modeled as:

$$\sigma_{\phi F}{}^2 = G^2 \int_0^\infty S_{U/L}(f) \cdot \left|1 - H_{U/L}(j2\pi f)\right|^2 \cdot \left|1 - H_{D/L}(j2\pi f)\right|^2 df, \tag{42}$$

DTF-21 and CTT-22

Equation (42) reflects the fact that uplink-carrier phase noise will largely be canceled by phase noise in the local oscillators of the receiving chain but that this cancellation is imperfect when the transponder does not track all of the uplink-carrier phase noise. The product $S_{U/L}(f) \cdot \left|1 - H_{U/L}(j2\pi f)\right|^2 \cdot \left|1 - H_{D/L}(j2\pi f)\right|^2$ represents that portion of the uplink-carrier phase noise that is not tracked by the transponder and not tracked by the DTT receiver. When the transponder's carrier-loop bandwidth B_{TR} and the DTT carrier-loop bandwidth B_L are large,

$\sigma_{\phi F}{}^2$ will be negligible. To the extent that B_{TR} and B_L are not sufficiently large, an estimate of $\sigma_{\phi F}{}^2$ requires a numerical evaluation of Equation (42).

2.3.4.2.3 Phase Scintillation Contribution to $\sigma_\phi{}^2$, Coherent

In two-way and three-way tracking, both the uplink and downlink carriers acquire phase scintillation when passing through the solar corona. During coherent operation, the uplink phase scintillation is transponded onto the downlink carrier.

The contribution $\sigma_{\phi S}{}^2$ of phase scintillation to downlink-carrier phase error variance may be approximated with Equation (35), which is repeated below for the reader's convenience.

$$\sigma_{\phi S}{}^2 = \begin{cases} \dfrac{C_{\text{band}} \cdot C_{\text{loop}}}{[\sin(\theta_{\text{SEP}})]^{2.45} \cdot B_L{}^{1.65}}, & 0^\circ < \theta_{\text{SEP}} \leq 90^\circ \\ \dfrac{C_{\text{band}} \cdot C_{\text{loop}}}{B_L{}^{1.65}}, & 90^\circ < \theta_{\text{SEP}} \leq 180^\circ \end{cases} \tag{35}$$

θ_{SEP} is the Sun-Earth-probe angle ($0^\circ < \theta_{\text{SEP}} \leq 180^\circ$). $\sigma_{\phi S}{}^2$ has the dimensions rad^2. (The product $C_{\text{band}} \cdot C_{\text{loop}}$ has the same dimensions as $B_L{}^{1.65}$.) The parameter C_{band} is constant for any given band pairing and is given by Equation (29), which is repeated below for the reader's convenience.

$$C_{\text{band}} = \begin{cases} 6.1 \times 10^{-5}, & \text{S} - \text{up/S} - \text{down} \\ 4.8 \times 10^{-4}, & \text{S} - \text{up/X} - \text{down} \\ 2.6 \times 10^{-5}, & \text{X} - \text{up/S} - \text{down} \\ 5.5 \times 10^{-6}, & \text{X} - \text{up/X} - \text{down} \\ 5.2 \times 10^{-5}, & \text{X} - \text{up/Ka} - \text{down} \\ 1.9 \times 10^{-6}, & \text{Ka} - \text{up/X} - \text{down} \\ 2.3 \times 10^{-7}, & \text{Ka} - \text{up/Ka} - \text{down} \end{cases} \tag{29}$$

The parameter C_{loop} is constant for a given loop and is given by Equation (36), which is repeated below for the reader's convenience.

$$C_{\text{loop}} = \begin{cases} 5.9, & \text{standard underdamped type 2 loop} \\ 5.0, & \text{supercritically damped type 2 loop} \\ 8.2, & \text{standard underdamped type 3 loop} \\ 6.7, & \text{supercritically damped type 3 loop} \end{cases} \tag{36}$$

Equation (35) indicates that $\sigma_{\phi S}{}^2$ increases as θ_{SEP} decreases and as B_L decreases.

Appendix A: Carrier-Loop Transfer Function

The transfer function of the DTT receiver's carrier loop is characterized here. For a type 2 loop, the transfer function is given by:

$$H_{D/L}(s) = \frac{K_1 s + K_2}{s^2 + K_1 s + K_2} \tag{43}$$

where s is the Laplace transform variable. The parameters K_1 and K_2 depend on whether the loop is standard underdamped or supercritically damped (Reference 12), as shown in Table 2.

Table 2. Type 2 Loop Parameters

	K_1	K_2
standard underdamped	$\frac{8}{3}B_L$	$\frac{1}{2}{K_1}^2$
supercritically damped	$\frac{16}{5}B_L$	$\frac{1}{4}{K_1}^2$

B_L is the one-sided, noise-equivalent bandwidth of the carrier loop (Hz).

$$B_L = \int_0^\infty \left|H_{D/L}(j2\pi f)\right|^2 df \tag{44}$$

For a type 3 loop, the transfer function is given by:

$$H_{D/L}(s) = \frac{K_1 s^2 + K_2 s + K_3}{s^3 + K_1 s^2 + K_2 s + K_3} \tag{45}$$

The parameters K_1, K_2 and K_3 depend on whether the loop is standard underdamped or supercritically damped (Reference 12), as shown in Table 3.

Table 3. Type 3 Loop Parameters

	K_1	K_2	K_3
standard underdamped	$\frac{60}{23}B_L$	$\frac{4}{9}{K_1}^2$	$\frac{2}{27}{K_1}^3$
supercritically damped	$\frac{32}{11}B_L$	$\frac{1}{3}{K_1}^2$	$\frac{1}{27}{K_1}^3$

Appendix B: Glossary of Parameters

$P_C/N_0\|_{D/L}$	downlink residual-carrier power to noise spectral density ratio, Hz
$P_T/N_0\|_{D/L}$	downlink total signal power to noise spectral density ratio, Hz
E_S/N_0	telemetry symbol energy to noise spectral density ratio
ρ_{TR}	signal-to-noise ratio of transponder's carrier loop
ρ_L	signal-to-noise ratio of DTT receiver's carrier loop
B_{TR}	noise-equivalent bandwidth of transponder's carrier-loop bandwidth, Hz
B_L	noise-equivalent bandwidth of DTT receiver's carrier loop, Hz
$H_{U/L}(j2\pi f)$	frequency response of transponder's carrier loop
$H_{D/L}(j2\pi f)$	frequency response of DTT receiver's carrier loop
$S_{U/L}(f)$	one-sided power spectral density of uplink-carrier phase noise, $\mathrm{rad}^2/\mathrm{Hz}$
$S_{D/L}(f)$	one-sided power spectral density of downlink-carrier phase noise, $\mathrm{rad}^2/\mathrm{Hz}$
S_L	squaring loss of a (BPSK) Costas loop
S_{LQ}	squaring loss of a QPSK or OQPSK loop
T	integration time for Doppler measurement, s
$T_{S\,(\mathrm{binary})}$	period of the binary symbol, s
R_{SYM}	telemetry symbol rate, symbols per second
f_C	downlink carrier frequency, Hz
c	speed of electromagnetic waves in vacuum, mm/s
G	transponding ratio
α	Doppler Rate, Hz/s
β	Doppler Acceleration, $\mathrm{Hz/s}^2$
θ_{SEP}	Sun-Earth-probe angle ($0^\circ < \theta_{\mathrm{SEP}} \leq 180^\circ$)
θ_t	telemetry modulation index, rad
I_{data}	data imbalance, $0 \leq I_{\mathrm{data}} \leq 0.5$
σ_f	standard deviation of frequency, Hz
σ_{VI}	standard deviation of Doppler error due to telemetry data imbalance, mm/s

$\sigma_y(T)$	Allan deviation
${\sigma_V}^2$	variance of range rate, $\mathrm{mm}^2/\mathrm{s}^2$
${\sigma_{VN}}^2$	contribution to ${\sigma_V}^2$ from white (thermal) noise, $\mathrm{mm}^2/\mathrm{s}^2$
${\sigma_{VF}}^2$	contribution to ${\sigma_V}^2$ from phase noise of frequency sources, $\mathrm{mm}^2/\mathrm{s}^2$
${\sigma_{VS}}^2$	contribution to ${\sigma_V}^2$ from (solar) phase scintillation, $\mathrm{mm}^2/\mathrm{s}^2$
${\sigma_\phi}^2$	carrier phase error variance, rad^2
${\sigma_{\phi N}}^2$	contribution to ${\sigma_\phi}^2$ from white (thermal) noise, rad^2
${\sigma_{\phi F}}^2$	contribution to ${\sigma_\phi}^2$ from phase noise of frequency sources, rad^2
${\sigma_{\phi S}}^2$	contribution to ${\sigma_\phi}^2$ from (solar) phase scintillation, rad^2
${\sigma_{\phi NU}}^2$	contribution to ${\sigma_{\phi N}}^2$ from uplink white (thermal) noise, rad^2
${\sigma_{\phi ND}}^2$	contribution to ${\sigma_{\phi N}}^2$ from downlink white (thermal) noise, rad^2

References

1. J. B. Berner and K. M. Ware, "An Extremely Sensitive Digital Receiver for Deep Space Satellite Communications," *Eleventh Annual International Phoenix Conference on Computers and Communications*, pp. 577-584, Scottsdale, Arizona, April 1-3,1992.

2. J. Lesh, "Tracking Loop and Modulation Format Considerations for High Rate Telemetry," *DSN Progress Report 42-44*, Jet Propulsion Laboratory, Pasadena, CA, pp. 117-124, April 15, 1978.

3. M. K. Simon and W. C. Lindsey, "Optimum Performance of Suppressed Carrier Receivers with Costas Loop Tracking," *IEEE Transactions on Communications*, Vol. COM-25, No. 2, pp. 215-227, February 1977.

4. J. H. Yuen, editor, *Deep Space Telecommunications Systems Engineering*, Plenum Press, New York, pp. 94-97, 1983.

5. C. L. Thornton and J. S. Border, *Radiometric Tracking Techniques for Deep-Space Navigation*, Monograph 1 of the *Deep-Space Communications and Navigation Series*, Jet Propulsion Laboratory, Pasadena, CA, 2000.

6. S. W. Asmar, J. W. Armstrong, L. Iess, and P. Tortora, “Spacecraft Doppler Tracking: Noise Budget and Accuracy Achievable in Precision Radio Science Observations,” *Radio Science*, Vol. 40, RS2001, 2005.

7. J. A. Barnes, *et al.*, “Characterization of Frequency Stability,” *IEEE Transactions on Instrumentation and Measurement*, Vol. IM-20, No. 2, pp. 105-120, May 1971.

8. R. Woo and J. W. Armstrong, "Spacecraft Radio Scattering Observations of the Power Spectrum of Electron Density Fluctuations in the Solar Wind," *Journal of Geophysical Research*, Vol. 84, No. A12, pp. 7288-7296, December 1, 1979.

9. D. D. Morabito, S. Shambayati, S. Finley, and D. Fort, “The Cassini May 2000 Solar Conjunction,” *IEEE Transactions on Antennas and Propagation*, Vol. 51, No. 2, pp. 201-219, February 2003.

10. A. Monk, "Carrier-to-Noise Power Estimation for the Block-V Receiver," *TDA Progress Report 42-106*, Jet Propulsion Laboratory, Pasadena, CA, pp. 353-363, August 15, 1991.

11. S. Dolinar, "Exact Closed-Form Expressions for the Performance of the Split-Symbol Moments Estimator of Signal-to-Noise Ratio," *TDA Progress Report 42-100*, pp. 174-179, Jet Propulsion Laboratory, Pasadena, CA, February 15, 1990.

12. S. A. Stephens and J. B. Thomas, "Controlled-Root Formulation for Digital Phase-Locked Loops," *IEEE Transactions on Aerospace and Electronic Systems*, Vol. 31, No. 1, pp. 78-95, January 1995.